Chemical Physics Letters 757 (2020) 137860

Contents lists available at ScienceDirect

Chemical Physics Letters

journal homepage: www.elsevier.com/locate/cplett

Research paper

Time-dependent density functional theory study of the X-ray emission spectroscopy of amino acids and proteins

Aleksandra Foerster, Nicholas A. Besley

School of Chemistry, University of Nottingham, University Park, Nottingham NG7 2RD, UK

HIGHLIGHTS

- Simulation of the non-resonant X-ray emission spectra of amino acids.
- Time-dependent density functional theory with the CAM-B3LYP functional provides accurate spectra.
- The dependence of the spectra on the geometry of the peptide bond studied for α-helix and β-sheets.

ARTICLE INFO

Keywords:
X-ray emission spectroscopy
Amino acids
Polypeptides
Density functional theory

ABSTRACT

The non-resonant X-ray emission spectroscopy of amino acids and a dipeptide have been studied using time-dependent density functional theory (TDDFT) calculations at the nitrogen and oxygen K-edges. Comparison with higher level calculations and experimental data shows that TDDFT with the CAM-B3LYP exchange–correlation functional and (Z + 1)6-311G* basis set provides an accurate description of the spectra. Calculations for model α-helix and β-sheet structures show the spectra to relatively insensitive to the structure of peptide bond, with the greatest variation observed at the oxygen K-edge.

1. Introduction

Amino acids are the fundamental building blocks of nature and combine together to form proteins, and this biological significance has led to an interest in understanding their geometrical and electronic structure. Spectroscopic methods are commonly used to probe the structure of oligopeptides and proteins [1]. Despite offering much lower resolution than solid-state X-ray diffraction, the fast timescales accessible to these techniques allows processes such as folding and unfolding processes to be studied [2,3]. Natural circular dichroism (CD) spectroscopy in the ultraviolet region is widely used in this regard since the different elements of secondary structure, helix, β-sheet and turn, have characteristic spectral profiles [1].

In recent years, spectroscopic techniques using X-rays have emerged as a powerful analytical tool driven by the increasing availability of synchrotron sources and free-electron lasers. This raises the question of whether spectroscopic measurements in the X-ray region are able to distinguish between different elements of secondary structure. There has been a number of studies on the X-ray absorption spectroscopy, or more specifically the near edge X-ray absorption fine structure (NEXAFS), of amino acids and small polypeptides [4–8]. It has been found that, in general, these spectra are not sufficiently different for chemical identification [4]. This work has been extended to consider protein secondary structure models, where it was concluded that there are relatively small differences in the computed NEXAFS spectra at the carbon and oxygen K-edges, with the greatest difference was predicted to occur at the nitrogen K-edge [9]. Other computational studies have considered X-ray natural circular dichroism (XNCD) of amino acids [10–14], including using the static-exchange (STEX) approximation [10] and the complex polarization propagation method in conjunction with density functional theory (DFT) [11,13]. It has been shown that XNCD has a greater sensitivity to the type of amino acid compared with X-ray absorption spectroscopy, and the potential to be a better technique to fingerprint these compounds.

The focus of this work is X-ray emission spectroscopy (XES), and the XES of glycine on the Cu(110) surface has been studied [15]. More recent work has probed the XES and resonant inelastic X-ray scattering (RIXS) of amino acids in aqueous solution [16–18] and the solid state [19,20]. In particular, Weinhardt and co-workers have presented a detailed characterisation of the XES and RIXS of amino acids. This includes a library of spectra for all proteinogenic amino acids [20], the development of a building block model [18] and the study of peptides [21].

In parallel with the advances in experimental measurements, there

E-mail address: nick.besley@nottingham.ac.uk (N.A. Besley).

https://doi.org/10.1016/j.cplett.2020.137860
Received 15 May 2020; Received in revised form 22 July 2020; Accepted 5 August 2020
Available online 10 August 2020
0009-2614/

has also been developments in the calculation of X-ray emission spectra using quantum chemical methods, such as Kohn–Sham density functional theory (DFT) and time-dependent density functional theory (TDDFT) [22,23]. These calculations can play an important role in enabling the understanding and interpretation of experimental data. In this Letter, we examine the accuracy of DFT-based methods for the simulation of X-ray emission spectra of amino acids, in particular assessing the relative accuracy of simulated spectra based upon DFT and TDDFT calculations. Subsequently TDDFT is applied to study the XES of polypeptides and fragments of protein secondary structure to investigate the dependence of the spectra on the structure of the peptide bond.

2. Computational methods

Non-resonant XES measures the emission following ionisation of a core electron, XES can also be performed under resonant conditions where the emission from a core-excited state, rather than core-ionised state, is measured. Within the framework of DFT, the transition energies and the associated intensities can be determined directly from the Kohn–Sham DFT calculation by approximating the transition energy as the energy difference between the orbital energies of the neutral ground state molecule

$$\Delta E = \epsilon_v - \epsilon_c \tag{1}$$

with the oscillator strength given by

$$f \propto |\langle \phi_c | \hat{\mu} | \phi_v \rangle|^2 \tag{2}$$

where ϕ_c is a core orbital and ϕ_v is a valence orbital. This approach takes no account of the orbital relaxation for the core-ionised state, but despite of this approximation, it has been applied successfully in a variety of applications, including the probing the chemical bonding of molecules on surfaces [24,25], valence-to-core XES of transition metal complexes [26,27] and the study of carbon nanostructures [28]. A semi-classical Kramers-Heisenberg (SCKH) approximation that captures vibrational interference effects has been developed [29], and applied to study liquids [30,31], and damped coupled-cluster response theory methods have also been developed [32]. XES can also be determined using TDDFT through the use of a reference determinant with a core–hole [33], and this approach has been used to study the valence-to-core XES of transition metal complexes [34–37] and water [38,39]. The advantage of this approach is that the core–hole relaxation is incorporated explicitly. This strategy of using a core–hole reference determinant is not limited to TDDFT calculations and has also been exploited within ADC [40] and EOM-CCSD formalisms [41]. An important consideration in these calculations is that the basis set is able to describe the core-ionised state [42]. Recently is has been proposed that the basis set be augmented through the addition of the core and valence (not polarisation) basis functions for the element with one higher nuclear charge [43]. This is only necessary for the element being ionised, and the resulting basis sets are termed (Z + 1) basis sets.

For both neutral (uncharged) and zwitterionic forms of glycine, X-ray emission spectra were computed for the nitrogen and oxygen K-edges using DFT (i.e. via Eqs. (1) and (2)) and TDDFT. The structure of glycine was optimised at the B3LYP/6-31G* level, and for the DFT spectra the long-range corrected CAM-B3LYP [44] and short-range corrected SRC1r1 [45] exchange–correlation functionals were used with 6-311G* basis set. TDDFT spectra were computed using the B3LYP [46] and CAM-B3LYP functionals and the (Z + 1)6-311G* basis set, where the additional basis functions were included only for the element being ionised. In these calculations the maximum overlap method [47] was used to maintain the core–hole during the DFT calculation. For comparison, spectra were also determined using the EOM-CCSD method with the (Z + 1)6-311G* basis set. Further TDDFT/CAM-B3LYP calculations for alanine, cysteine and proline were performed using a similar approach. All of the calculations on the zwitterionic forms of the amino acids used the polarised continuum model (PCM) [48] with a dielectric constant of 78.39. Spectra have also been computed that include averaging over structures generated from an ab initio molecular dynamics (AIMD) simulation of the core-ionised state. These calculations sample 50 structures extracted at uniform time intervals from a 5 fs (which reflects the typical lifetime of the core-ionised state [49]) AIMD simulation using the CAM-B3LYP functional and (Z + 1)6-311G* basis set for the appropriate core-ionised state. Spectra have been generated by convoluting the calculated transition energies and intensities with gaussian functions with full-width at half maximum (FWHM) of 0.25 eV, which accounts for many factors such as shake-up and Auger processes that are not described by the calculations. This FWHM is chosen to provide a visual representation of the computed spectra and has not been optimised to fit the experimental data.

3. Results and discussion

Despite its small size, the molecular structure of glycine shows a complex behaviour. In the gas-phase the carboxylic acid (COOH) and amino (NH_2) groups are uncharged, which we refer to as the neutral form, while in the solid state glycine exists as the zwitterionic form (COO^- and NH_3^+). In solution the charge state of the carboxylic acid and amino groups depends on the pH of the solution. Figs. 1 and 2 show the computed X-ray emission spectra for the zwitterionic and neutral forms of glycine determined with a range of computational approaches. The formally most accurate method used is EOM-CCSD/(Z + 1)6-311G* and the corresponding spectra are used as a benchmark to assess the DFT-based calculations. The transition energies calculated using DFT and TDDFT show a wide variation, from being systematically too high to systematically too low. This is expected, and has been discussed previously in the literature [27,33]. As a consequence, in Figs. 1 and 2

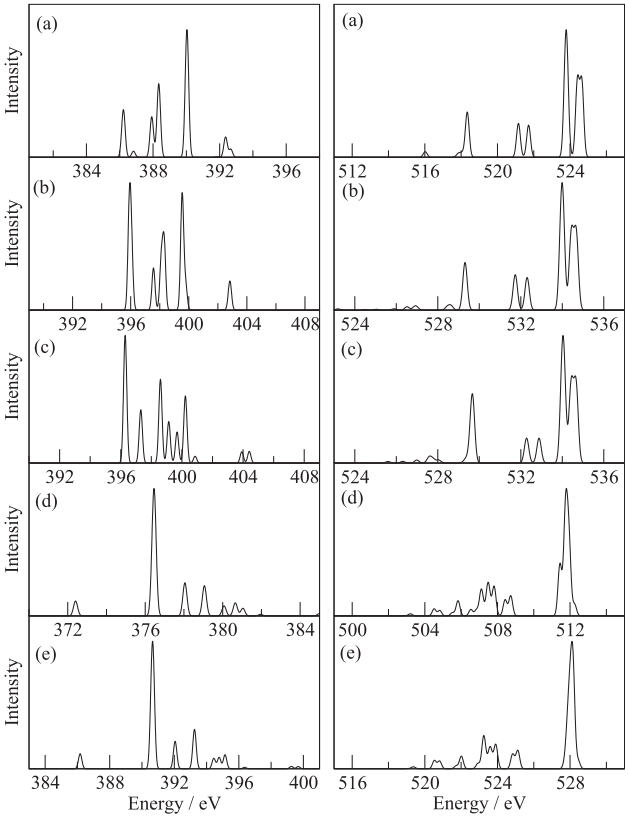

Fig. 1. Calculated non-resonant X-ray emission spectra the zwitterionic form of glycine at the nitrogen K-edge (left) and oxygen K-edge (right). (a) EOM-CCSD/(Z + 1)6-311G* (b) TDDFT-CAM-B3LYP/(Z + 1)6-311G* (c) TDDFT-B3LYP/(Z + 1)6-311G* (d) DFT-CAM-B3LYP/6-311G* (e) DFT-CAM-SRC1r1/6-311G*.

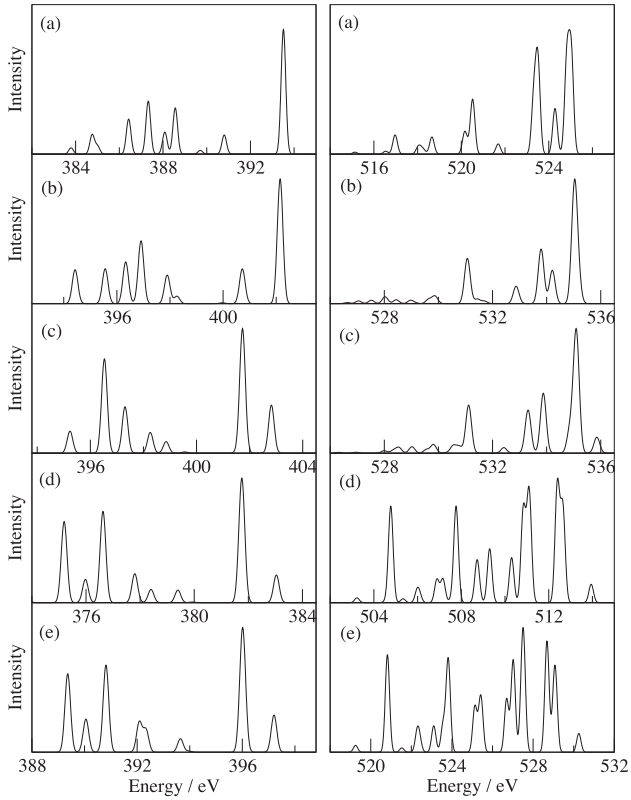

Fig. 2. Calculated non-resonant X-ray emission spectra the neutral form of glycine at the nitrogen K-edge (left) and oxygen K-edge (right). (a) EOM-CCSD/(Z+1)6-311G* (b) TDDFT-CAM-B3LYP/(Z+1)6-311G* (c) TDDFT-B3LYP/(Z+1)6-311G* (d) DFT-CAM-B3LYP/6-311G* (e) DFT-CAM-SRC1r1/6-311G*.

the spectra have been shifted in energy to align with the EOM-CCSD spectra and we focus on the ability of the DFT-based methods to describe the spectral profile correctly, with the understanding that a constant energy shift can be applied to align the spectra with experiment.

For both the nitrogen and oxygen K-edge, the spectra computed directly from the DFT calculation using the CAM-B3LYP and SRC1r1 functionals show the greatest deviation from the EOM-CCSD spectra, and overall provide a poor description for both neutral and zwitterionic forms. The spectra predicted by the two functionals, which are very different in nature, are similar to each other suggesting that the source of the observed discrepancy is the approach for determining the transition energies and intensities rather than the functionals themselves. In particular for the zwitterionic form the calculated intensity is low for the higher energy bands in the nitrogen K-edge spectra, which is not consistent with experiment (see later). This has also been observed in previous calculations [17], although this was improved through the consideration of effects of molecular dynamics along the core-ionised trajectory.

The nitrogen and oxygen K-edge spectra computed using TDDFT show a closer agreement with the EOM-CCSD spectra. This is perhaps not surprising since there is a much greater similarity in the approaches to determining the spectra. A closer examination of the spectra for the two functionals shows that there is little variation between the calculated spectra at the oxygen K-edge, while there is significant differences for the nitrogen K-edge where CAM-B3LYP provides a significantly better description of the EOM-CCSD spectra. This is consistent with recent work that found CAM-B3LYP to give accurate spectra for a range of organic molecules in a comparison with experimental data [50]. In particular, for the nitrogen K-edge of the zwitterionic form CAM-B3LYP and EOM-CCSD methods predict high intensity for the higher energy bands, in contrast to the B3LYP spectrum. The agreement between

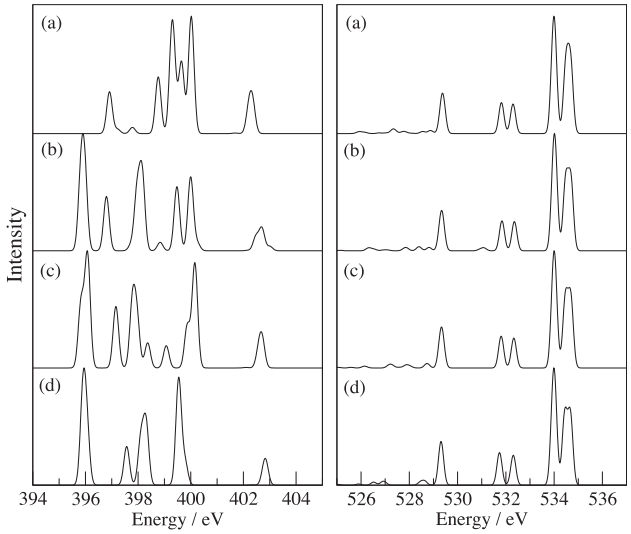

Fig. 3. Calculated TDDFT/CAM-B3LYP non-resonant X-ray emission spectra the zwitterionic forms of (a) proline, (b) cysteine, (c) alanine and (d) glycine at the nitrogen K-edge (left) and oxygen K-edge (right).

CAM-B3LYP and EOM-CCSD for the neutral form is slightly poorer than for the zwitterionic form, however, the discrepancy is primarily associated with the predicted intensities rather than the relative energy of the bands.

It is also important to compare the computed spectra with experimental data. Experimental measurements have been reported for the 20 most common proteingenic amino acids in their solid zwitterionic forms [20], and as a consequence we focus on the zwitterionic forms of the amino acids. The calculations on glycine suggest that the TDDFT/CAM-B3LYP approach provides a good description of the EOM-CCSD spectra. This is significant since the lower computational cost of TDDFT means that this approach can be readily applied to study larger systems. Fig. 3 shows computed TDDFT/CAM-B3LYP spectra for glycine, alanine, cysteine and proline. The resulting spectra show that at the oxygen K-edge there is little variation between the spectra for the different amino acids. This is consistent with the experimental observations and reflects the nature of the COO^- group which is relatively unaffected by the changes in the amino acid structure. For the nitrogen K-edge there are only small variations in the spectra for glycine, alanine and cysteine, but there is a significant change for proline which results from the changing nature of the bonding to nitrogen in proline, where the amino group is part of the heterocycle, in contrast to the other amino acids.

Fig. 4 shows a direct comparison for glycine and proline of the computed TDDFT/CAM-B3LYP spectra with experimental spectra, which have been adapted from reference [20]. In this comparison experimental spectra for the solid state are compared with spectra computed for a single molecule with the PCM describing the extended environment, so some variations may be expected, however, these differences are expected to be small [21]. An energy shift has been applied to the computed spectra to align the most intense bands with experiment, which results in a shift of −4.8 eV for nitrogen K-edge and −7.4 eV for the oxygen K-edge spectra.

Initially we consider the spectra computed based upon the single ground state molecular structure. The oxygen K-edge spectra are in good agreement with the experimental data for both glycine and proline. The largest discrepancy is for the peak labelled 3 which is too low in energy and only appears as a small shoulder in the experimental data. The molecular orbitals associated with the observed bands are shown in the Supporting Information. The intense band that dominates the experimental spectra comprises two components from orbitals with oxygen lone pair or π character at the carboxylic group, but crucially these orbitals have atomic p-orbital character around the oxygen atoms

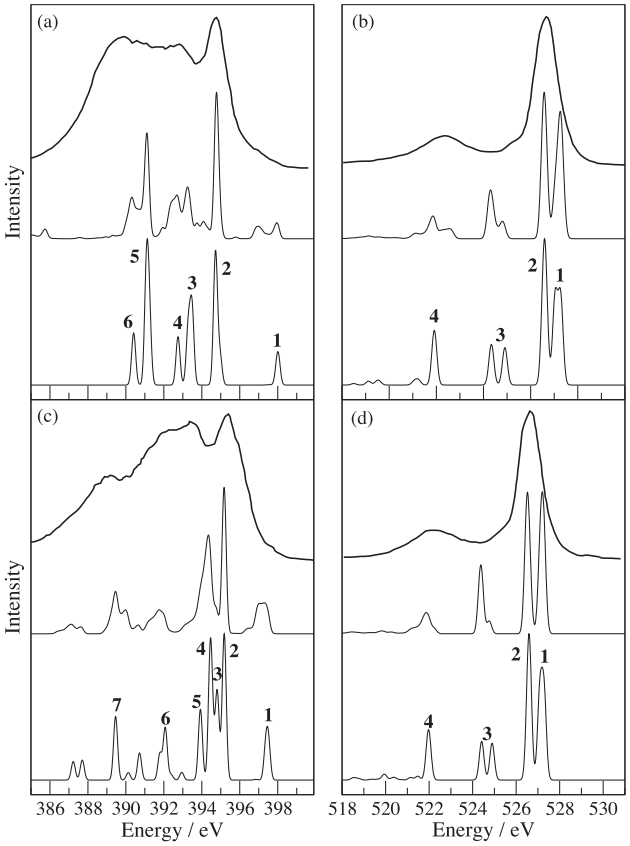

Fig. 4. Experimental and calculated TDDFT/CAM-B3LYP non-resonant X-ray emission spectra the zwitterionic forms of (a) nitrogen K-edge glycine, (b) oxygen K-edge glycine, (c) nitrogen K-edge proline and (d) oxygen K-edge proline. Upper spectra: experiment adapted from reference [20], middle spectra: calculated spectra including molecular dynamics and lower spectra: static (single structure) calculated spectra. An energy shift of −4.8 eV for nitrogen and −7.4 eV for oxygen have been applied to the calculated spectra to align them with experiment.

consistent with the large intensity for the transition to the oxygen 1s orbital.

The nitrogen K-edge spectra are more complex with a large number of transitions contributing to the broad band observed in experiment. However, in general the calculations predict bands that align with the distinct features observed in experiment. The peak labelled 1 corresponds to orbitals that are predominantly localised on the carboxylic acid group, and there is some evidence of a weak feature in the experimental spectra at this energy. For glycine, bands 2 and 5 are the most intense and arise from σ and π-type orbitals localised on the amino group. Also shown are spectra that incorporate the nuclear motions that occur on the femtosecond timescale in the core-ionised state. This leads to a relatively small change for the oxygen K-edge spectra, but larger changes are observed for the nitrogen K-edge leading to an improved agreement with the experimental data.

Diglycine represents a simple system that contains the peptide bond. Fig. 5 shows the computed nitrogen and oxygen K-edge TDDFT with CAM-B3LYP spectra for the zwitterionic form of diglycine along with the experimental data from reference [21]. To align the calculated spectra with experiment energy shifts of −6.6 eV and −7.3 eV have been applied for nitrogen and oxygen, respectively. The agreement between the computed spectra and experiment is very good. Fig. 5 also shows the contribution to the spectra from the different nitrogen and oxygen atoms. For this purpose the two oxygen atoms of the COO^- group are treated together. The most intense peak at the nitrogen K-edge is associated with the nitrogen atom of the peptide bond. This

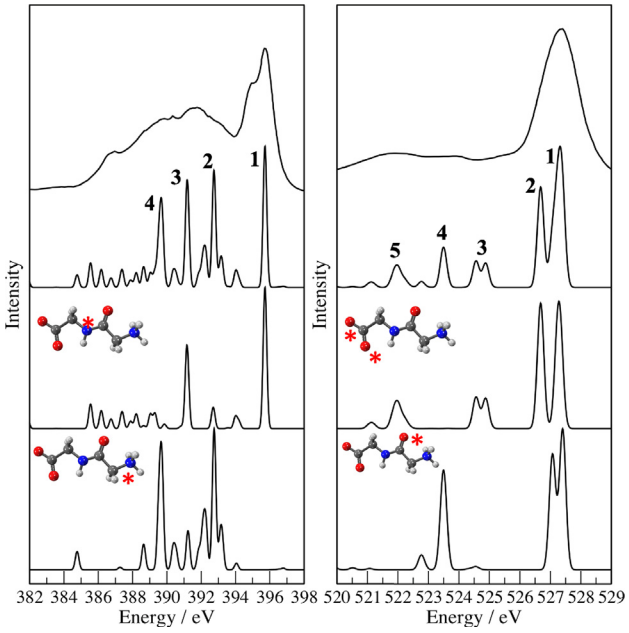

Fig. 5. Experimental and calculated TDDFT/CAM-B3LYP non-resonant X-ray emission spectra the zwitterionic form diglycine. Upper spectra: experiment adapted from reference [21]. The total computed spectrum and the contributions from the different nitrogen and oxygen atoms (indicated by an asterisk) are shown. An energy shift of −6.6 eV for nitrogen and −7.3 eV for oxygen has been applied to the calculated spectra to align them with experiment.

band arises from a π orbital on the peptide group that has a node between the carbon and the nitrogen, these orbitals are shown in the Supporting Information. The peptide nitrogen also contributes a peak at higher energy from orbitals that have σ character around the nitrogen atom. Two peaks (2 and 4) from the amino nitrogen are also evident in the spectrum. The orbitals associated with these peaks are similar in character to the orbitals that lead to the two most intense peaks in the spectrum for the zwitterionic form of glycine. For the oxygen K-edge spectra, the calculations show that both carbonyl and carboxylic acid group oxygens contribute to the dominant intense feature observed in the spectrum and the transitions arise from oxygen lone pair and π orbitals.

The biological significance of amino acids lies in their role in the structure of proteins. Previous computational studies have examined the near-edge X-ray absorption spectroscopy of different elements of protein secondary structure [9]. The computational cost of the TDDFT approach used here allows the study of quite large systems, and Figs. 6 and 7 show calculated spectra for model α-helix and β-sheet structures. The α-helix contains ten glycine residues with ψ/ϕ angles of -57° and -48° and the computed spectra only considers core-ionisation occurring on the four central residues. The β-sheet structure has been extracted from the agitoxin protein (PDB code: 1AGT) with the side chains removed, and transitions associated with the end residues are not included. These structures are considered in isolation and the effects of solvent are not included. However, these calculations provide some insight into the sensitivity of XES to the structural variation of the peptide bond that occurs in the different elements of protein structure.

The nitrogen K-edge spectrum for the α-helix shows one intense band which corresponds to the transition from a π-orbital localised on the same residue as the core-ionised nitrogen atom. This transition is similar to the one observed for diglycine. This peak will contain analogous contributions from all of the residues, which may occur at slightly different energies in a real helix. This is illustrated in Fig. S7 in the Supporting Information which shows the separate contributions to the calculated spectra from the core–hole located at the different nitrogen atoms. At lower energies are several weaker bands. The peak

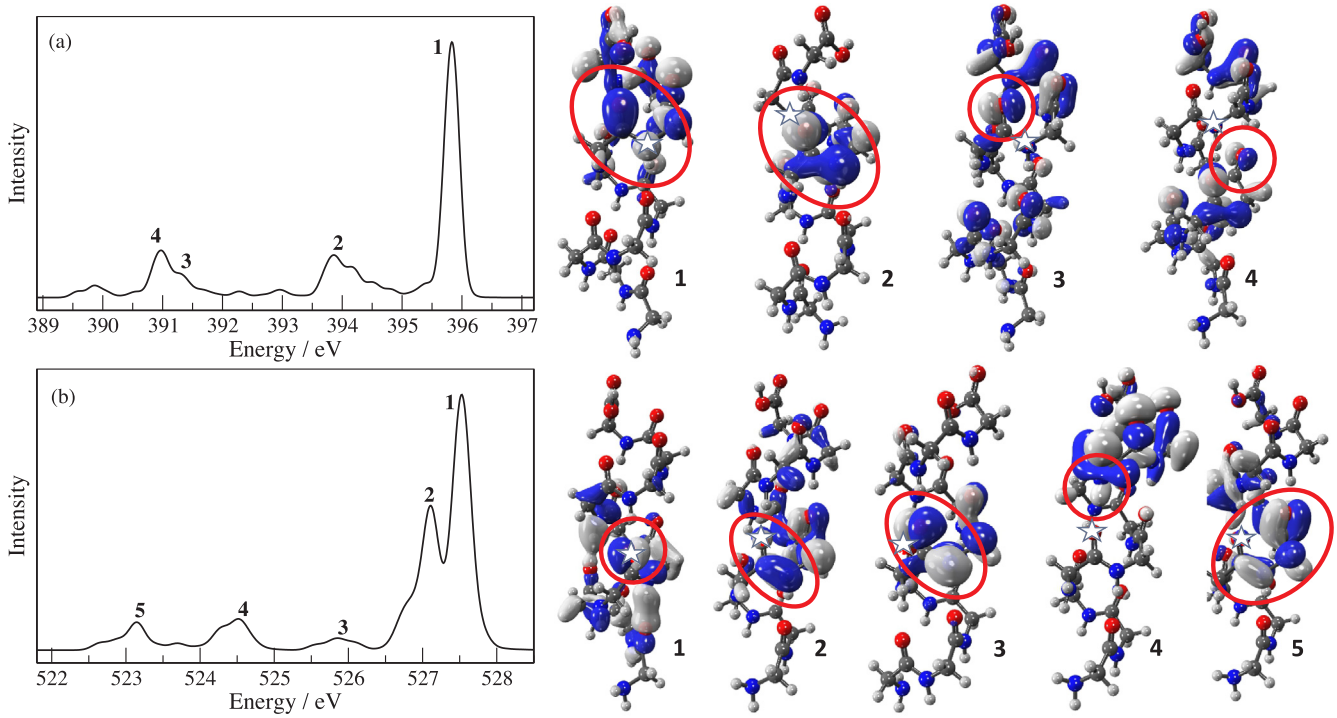

Fig. 6. Calculated non-resonant X-ray emission spectra for a model α-helix at the (a) nitrogen K-edge and (b) oxygen K-edge. Representative molecular orbitals associated with the labelled peaks are shown, where the star indicates the site of the core–hole in the initial state. An energy shift of -6.6 eV for nitrogen and -7.3 eV for oxygen has been applied to the calculated spectra.

labelled 2 arises from a transition from the π orbital on a neighbouring residue, while the remaining bands arise from transitions from oxygen lone pair orbitals on the same residue or on hydrogen bonded oxygen atoms. A similar analysis can be applied to the oxygen K-edge spectrum. The intense peaks (1 and 2) correspond to transitions from lone pair and π-orbitals localised on the same residue as the site of the core ionisation. Again the weaker peaks that lie at lower energies arise from transitions from neighbouring residues, this includes π-orbitals and orbitals associated with the hydrogen bonding N-H group.

The nitrogen K-edge spectrum for the β-sheet is qualitatively similar

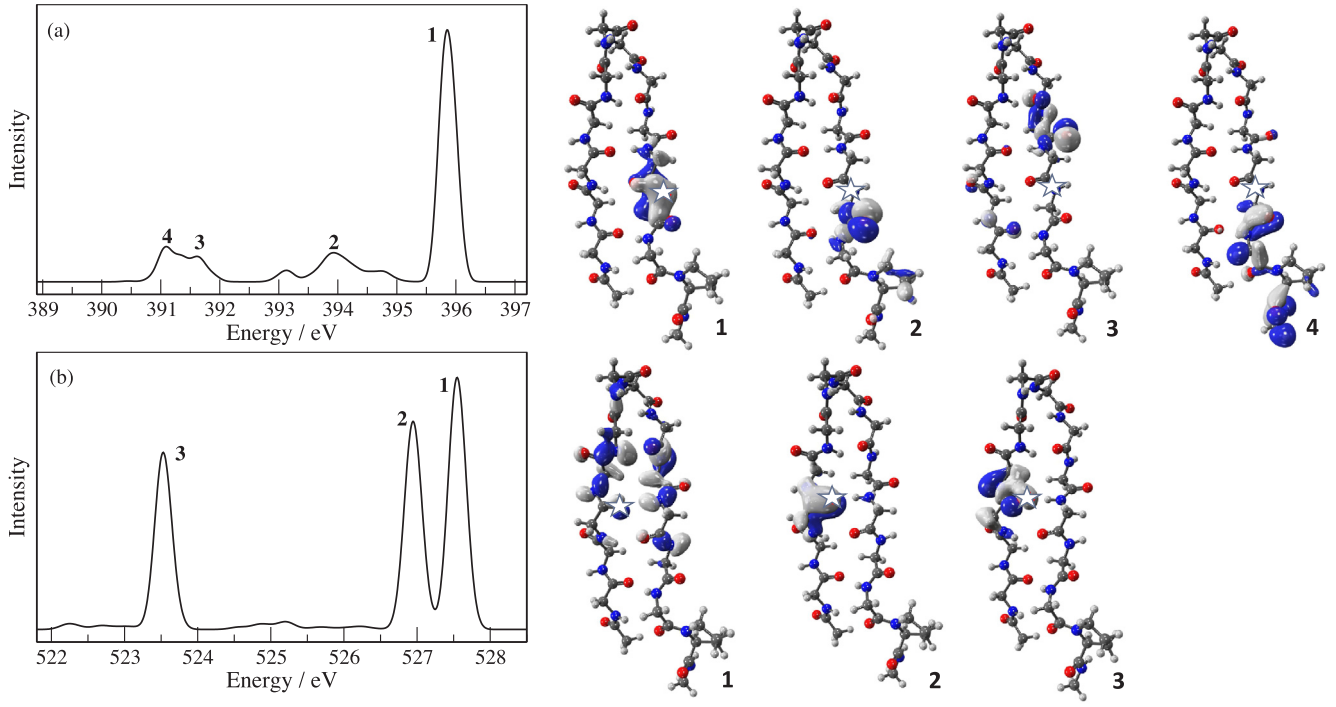

Fig. 7. Calculated non-resonant X-ray emission spectra for a β-sheet at the (a) nitrogen K-edge and (b) oxygen K-edge. Representative molecular orbitals associated with the labelled peaks are shown, where the star indicates the site of the core–hole in the initial state. An energy shift of -6.6 eV for nitrogen and -7.3 eV for oxygen has been applied to the calculated spectra.

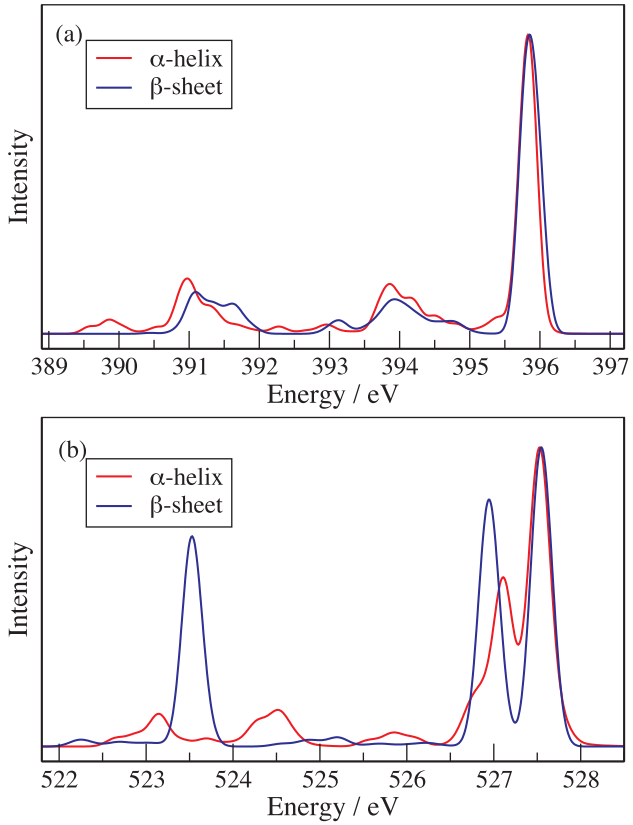

Fig. 8. Comparison of the calculated non-resonant X-ray emission spectra for the α-helix and β-sheet at the (a) nitrogen K-edge and (b) oxygen K-edge. An energy shift of -6.6 eV for nitrogen and -7.3 eV for oxygen has been applied to the calculated spectra.

to the one for the α-helix. The intense peak arises from a transition from a π orbital localised on the residue which is the site of the core-ionisation and the weaker peaks at higher energies are associated with transitions from orbitals on neighbouring residues. The separate contributions to the total spectrum from the core–hole localised on different atoms is shown in the Supporting Information. The oxygen K-edge spectra for the β-sheet shows some notable differences compared with the α-helix, with the lower energy peaks having significantly greater intensity. For this structure, all of the transitions arise from orbitals on the residue that has been core-ionised. A direct comparison between the spectra for the α-helix and β-sheet is shown in Fig. 8. This shows very little variation in the spectra a the nitrogen K-edge, but greater variation in the higher energy bands at the oxygen K-edge.

4. Conclusions

The X-ray emission spectra of amino acids, a dipeptide and model α-helix and β-sheet structures have been simulated using DFT-based approaches. Comparison with higher level calculations and experiment shows that TDDFT with the CAM-B3LYP exchange–correlation functional and (Z + 1)6-311G* basis set provides the most accurate description of the spectra of the methods studied. This approach has been applied to study model α-helix and β-sheet structures in order to probe the sensitivity of the spectra to the geometric structure of the peptide bond. The calculations show that the spectra for the α-helix and β-sheet are dominated by intense bands arising from transitions from orbitals that are localised on the residue that is the site of the core–hole, and transitions from orbitals on neighbouring residues lead to weaker peaks at lower energies. At the nitrogen K-edge there is no significant variation between the calculated spectra for the α-helix and β-sheet structures, while at the oxygen K-edge there is some variation in the intensity of the bands at higher energies.

CRediT authorship contribution statement

Aleksandra Foerster: Investigation, Formal analysis, Writing - review & editing. **Nicholas A. Besley:** Conceptualization, Writing - original draft, Supervision.

Declaration of Competing Interest

The authors declare that they have no known competing financial interests or personal relationships that could have appeared to influence the work reported in this paper.

Acknowledgements

The authors would like to thank the University of Nottingham for access to its High Performance Computing facility.

Appendix A. Supplementary material

Supplementary data associated with this article can be found, in the online version, at https://doi.org/10.1016/j.cplett.2020.137860.

References

[1] S.M. Kelly, T.J. Jess, N.C. Price, How to study proteins by circular dichroism, BBA – Proteins Proteomics 1751 (2005) 119–139.
[2] M. Buck, S.E. Radford, C.M. Dobson, A partially folded state of hen egg white lysozyme in trifluoroethanol: structural characterization and implications for protein folding, Biochemistry 32 (1993) 669–678.
[3] L. Nielsen, R. Khurana, A. Coats, S. Frokjaer, J. Brange, S. Vyas, V.N. Uversky, A.L. Fink, Effect of environmental factors on the kinetics of insulin fibril formation: elucidation of the molecular mechanism, Biochemistry 40 (2001) 6036–6046.
[4] K. Kaznacheyev, A. Osanna, C. Jacobsen, O. Plashkevych, O. Vahtras, H. Ågren, V. Carravetta, A.P. Hitchcock, Innershell absorption spectroscopy of amino acids, J. Phys. Chem. A 106 (2002) 3153–3168.
[5] M.L. Gordon, G. Cooper, C. Morin, T. Araki, C.C. Turci, K. Kaznatcheev, A.P. Hitchcock, Inner-shell excitation spectroscopy of the peptide bond: comparison of the C 1s, N 1s, and O 1s spectra of glycine, glycyl-glycine, and glycyl-glycyl-glycine, J. Phys. Chem. A 107 (2003) 6144–6159.
[6] O. Plekan, V. Feyer, R. Richter, M. Coreno, M. de Simone, K. Prince, V. Carravetta, An X-ray absorption study of glycine, methionine and proline, J. Elec. Spect. Rel. Phenom. 155 (2007) 47–53.
[7] V. Feyer, O. Plekan, R. Richter, M. Coreno, K.C. Prince, V. Carravetta, Photoemission and photoabsorption spectroscopy of glycyl-glycine in the gas phase, J. Phys. Chem. A 113 (2009) 10726–10733.
[8] C.P. Schwartz, R.J. Saykally, D. Prendergast, An analysis of the NEXAFS spectra of a molecular crystal: α-glycine, J. Chem. Phys. 133 (2010) 044507.
[9] M.W. Buckley, N.A. Besley, A theoretical study of the near edge X-ray absorption fine structure of amino acids and proteins, Chem. Phys. Lett. 501 (2011) 540–546.
[10] L. Yang, O. Plashkevych, O. Vahtras, V. Carravetta, H. Ågren, Near edge X-ray absorption and dichroism in amino acids, J. Synchrotron Rad. 6 (1999) 708–710.
[11] A. Jiemchooroj, U. Ekström, P. Norman, Near-edge x-ray absorption and natural circular dichroism spectra of l-alanine: a theoretical study based on the complex polarization propagator approach, J. Chem. Phys. 127 (2007) 165104.
[12] V. Kimberg, N. Kosugi, Calculation of K-edge circular dichroism of amino acids: comparison of random phase approximation with other methods, J. Chem. Phys. 126 (2007) 245101.
[13] S. Villaume, P. Norman, On circular dichroism and the separation between chromophore and chiral center: the near carbon K-edge X-ray absorption and circular dichroism spectra of noradrenaline and L-DOPA, Chirality 21 (2009) E13–E19.
[14] O. Takahashi, M. Kimoto, L.G. Pettersson, Theoretical study of the X-ray natural circular dichroism of some crystalline amino acids, Chem. Phys. 450–451 (2015) 109–114.
[15] A. Nilsson, N. Wassdahl, M. Weinelt, O. Karis, T. Wiell, P. Bennich, J. Hasselström, A. Föhlisch, J. Stöhr, M. Samant, Local probing of the surface chemical bond using x-ray emission spectroscopy, Appl. Phys. A 65 (1997) 147–154.
[16] J. Gråsjö, E. Andersson, J. Forsberg, L. Duda, E. Henke, W. Pokapanich, O. Björneholm, J. Andersson, A. Pietzsch, F. Hennies, J.-E. Rubensson, Local electronic structure of functional groups in glycine as anion, zwitterion, and cation in aqueous solution, J. Phys. Chem. B 113 (2009) 16002–16006.
[17] M. Blum, M. Odelius, L. Weinhardt, S. Pookpanratana, M. Bär, Y. Zhang, O. Fuchs, W. Yang, E. Umbach, C. Heske, Ultrafast proton dynamics in aqueous amino acid solutions studied by resonant inelastic soft X-ray scattering, J. Phys. Chem. B 116 (2012) 13757–13764.
[18] F. Meyer, M. Blum, A. Benkert, D. Hauschild, S. Nagarajan, R.G. Wilks,

J. Andersson, W. Yang, M. Zharnikov, M. Bär, C. Heske, F. Reinert, L. Weinhardt, Building block picture of the electronic structure of aqueous cysteine derived from resonant inelastic soft X-ray scattering, J. Phys. Chem. B 118 (2014) 13142–13150.
[19] F. Meyer, L. Weinhardt, M. Blum, M. Bär, R.G. Wilks, W. Yang, C. Heske, F. Reinert, Non-equivalent carbon atoms in the resonant inelastic soft X-ray scattering map of cysteine, J. Chem. Phys. 138 (2013) 034306.
[20] F. Meyer, M. Blum, A. Benkert, D. Hauschild, Y.L. Jeyachandran, R.G. Wilks, W. Yang, M. Bär, C. Heske, F. Reinert, M. Zharnikov, L. Weinhardt, X-ray emission spectroscopy of proteinogenic amino acids at all relevant absorption edges, J. Phys. Chem. B 121 (2017) 6549–6556.
[21] L. Weinhardt, A. Benkert, F. Meyer, M. Blum, D. Hauschild, R.G. Wilks, M. Bär, W. Yang, M. Zharnikov, F. Reinert, C. Heske, Local electronic structure of the peptide bond probed by resonant inelastic soft x-ray scattering, Phys. Chem. Chem. Phys. 21 (2019) 13207–13214.
[22] N.A. Besley, F.A. Asmuruf, Time-dependent density functional theory calculations of the spectroscopy of core electrons, Phys. Chem. Chem. Phys. 12 (2010) 12024–12039.
[23] P. Norman, A. Dreuw, Simulating X-ray spectroscopies and calculating core-excited states of molecules, Chem. Rev. 118 (2018) 7208–7248.
[24] A. Nilsson, J. Hasselström, A. Föhlisch, O. Karis, L. Pettersson, M. Nyberg, L. Triguero, Probing chemical bonding in adsorbates using x-ray emission spectroscopy, J. Elec. Spect. Rel. Phenom. 110–111 (2000) 15–39.
[25] A. Nilsson, L.G.M. Pettersson, Chemical bonding on surfaces probed by X-ray emission spectroscopy and density functional theory, Surf. Sci. Rep. 55 (2004) 49–167.
[26] N. Lee, T. Petrenko, U. Bergmann, F. Neese, S. DeBeer, Probing valence orbital composition with iron $K\beta$X-ray emission spectroscopy, J. Am. Chem. Soc. 132 (2010) 9715–9727.
[27] M.W.D. Hanson-Heine, M.W. George, N.A. Besley, Kohn-sham density functional theory calculations of non-resonant and resonant X-ray emission spectroscopy, J. Chem. Phys. 146 (2017) 094106.
[28] M.W. Hanson-Heine, M.W. George, N.A. Besley, Density functional theory calculations of the non-resonant and resonant X-ray emission spectroscopy of carbon fullerenes and nanotubes, Chem. Phys. Lett. 696 (2018) 119–124.
[29] M.P. Ljungberg, A. Nilsson, L.G.M. Pettersson, Semiclassical description of nuclear dynamics in X-ray emission of water, Phys. Rev. B 82 (2010) 245115.
[30] M.P. Ljungberg, I. Zhovtobriukh, O. Takahashi, L.G.M. Pettersson, Core-hole-induced dynamical effects in the S-ray emission spectrum of liquid methanol, J. Chem. Phys. 146 (2017) 134506.
[31] O. Takahashi, M.P. Ljungberg, L.G.M. Pettersson, X-ray emission spectrum of liquid ethanol: origin of split peaks, J. Phys. Chem. B 121 (2017) 11163–11168.
[32] R. Faber, S. Coriani, Resonant inelastic X-ray scattering and nonesonant x-ray emission spectra from coupled-cluster (damped) response theory, J. Chem. Theory Comput. 15 (2019) 520–528.
[33] J.D. Wadey, N.A. Besley, Quantum chemical calculations of x-ray emission spectroscopy, J. Chem. Theory Comput. 10 (2014) 4557–4564.
[34] Y. Zhang, S. Mukamel, M. Khalil, N. Govind, Simulating valence-to-core x-ray emission spectroscopy of transition metal complexes with time-dependent density functional theory, J. Chem. Theory Comp. 11 (2015) 5804–5809.
[35] I.P. Roper, N.A. Besley, The effect of basis set and exchange-correlation functional on time-dependent density functional theory calculations within the tamm-dancoff approxi mation of the X-ray emission spectroscopy of transition metal complexes, J. Chem. Phys. 144 (2016) 114104.
[36] D.R. Mortensen, G.T. Seidler, J.J. Kas, N. Govind, C.P. Schwartz, S. Pemmaraju, D.G. Prendergast, Benchmark results and theoretical treatments for valence-to-core X-ray emission spectroscopy in transition metal compounds, Phys. Rev. B 96 (2017) 125136.
[37] C.J. Clarke, S. Hayama, A. Hawes, J.P. Hallett, T.W. Chamberlain, K.R.J. Lovelock, N.A. Besley, Zinc 1s valence-to-core X-ray emission spectroscopy of halozincate complexes, J. Phys. Chem. A 123 (2019) 9552–9559.
[38] A.E.A. Fouda, G.I. Purnell, N.A. Besley, Simulation of ultra-fast dynamics effects in resonant inelastic X-ray scattering of gas-phase water, J. Chem. Theory Comput. 14 (2018) 2586–2595.
[39] I. Zhovtobriukh, N.A. Besley, T. Fransson, A. Nilsson, L.G.M. Pettersson, Relationship between X-ray emission and absorption spectroscopy and the local h-bond environment in water, J. Chem. Phys. 148 (2018) 144507.
[40] T. Fransson, A. Dreuw, Simulating X-ray emission spectroscopy with algebraic diagrammatic construction schemes for the polarization propagator, J. Chem. Theory Comput. 15 (2019) 546–556.
[41] N.A. Besley, Equation of motion coupled cluster theory calculations of the X-ray emission spectroscopy of water, Chem. Phys. Lett. 542 (2012) 42–46.
[42] A.E.A. Fouda, N.A. Besley, Assessment of basis sets for density functional theory-based calculations of core-electron spectroscopies, Theor. Chem. Acc. 137 (2017) 6.
[43] M.W. Hanson-Heine, M.W. George, N.A. Besley, Basis sets for the calculation of core-electron binding energies, Chem. Phys. Lett. 699 (2018) 279–285.
[44] T. Yanai, D.P. Tew, N.C. Handy, A new hybrid exchange-correlation functional using the coulomb-attenuating method (CAM-B3LYP), Chem. Phys. Lett. 393 (2004) 51–57.
[45] N.A. Besley, M.J.G. Peach, D.J. Tozer, Time-dependent density functional theory calculations of near-edge X-ray absorption fine structure with short-range corrected functionals, Phys. Chem. Chem. Phys. 11 (2009) 10350–10358.
[46] P.J. Stephens, F.J. Devlin, C.F. Chabalowski, M.J. Frisch, Ab initio calculation of vibrational absorption and circular dichroism spectra using density functional force fields, J. Phys. Chem. 98 (1994) 11623–11627.
[47] A.T.B. Gilbert, N.A. Besley, P.M.W. Gill, Self-consistent field calculations of excited states using the maximum overlap method (MOM), J. Phys. Chem. A 112 (2008) 13164–13171.
[48] J. Tomasi, B. Mennucci, R. Cammi, Quantum mechanical continuum solvation models, Chem. Rev. 105 (2005) 2999–3094.
[49] A. Lindgren, M. Gisselbrecht, F. Burmeister, A. Naves de Brito, A. Kivimäki, S.L. Sorensen, Molecular alignment of ammonia studied by electron-ion-ion coincidence spectroscopy, J. Chem. Phys. 122 (2005) 114306.
[50] A.E.A. Fouda, N.A. Besley, Improving the predictive quality of time-dependent density functional theory calculations of the X-ray emission spectroscopy of organic molecules, J. Comp. Chem. 41 (2020) 1081–1090.